Journal of Rock Mechanics and Geotechnical Engineering 8 (2016) 398–404

Contents lists available at ScienceDirect

Journal of Rock Mechanics and Geotechnical Engineering

journal homepage: www.rockgeotech.org

Full length article

Long-term stability analysis of the left bank abutment slope at Jinping I hydropower station

Long Zhang [a,*], Qiang Yang [b], Yaoru Liu [b]

[a] Beijing Urban Construction Design & Development Group Co., Ltd., Beijing, China
[b] State Key Laboratory of Hydroscience and Engineering, Tsinghua University, Beijing, China

ARTICLE INFO

Article history:
Received 29 April 2015
Received in revised form
17 July 2015
Accepted 24 August 2015
Available online 4 April 2016

Keywords:
Creep model
Long-term stability
Jinping I hydropower station
Abutment slope

ABSTRACT

The time-dependent behavior of the left bank abutment slope at Jinping I hydropower station has a major influence on the normal operation and long-term safety of the hydropower station. To solve this problem, a geomechanical model containing various faults and weak structural planes is established, and numerical simulation is conducted under normal water load condition using FLAC^{3D}, incorporating creep model proposed based on thermodynamics with internal state variables theory. The creep deformations of the left bank abutment slope are obtained, and the changes of principal stresses and deformations of the dam body are analyzed. The long-term stability of the left bank abutment slope is evaluated according to the integral curves of energy dissipation rate in domain and its derivative with respect to time, and the non-equilibrium evolution rules and the characteristic time can also be determined using these curves. Numerical results show that the left bank abutment slope tends to be stable in a global sense, and the stress concentration is released. It is also indicated that more attention should be paid to some weak regions within the slope in the long-term deformation process.

1. Introduction

The time-dependent deformation of rock mass is inevitable when a preexisting equilibrium of rock mass is disturbed by excavation, impounding, etc (Fakhimi and Fairhurst, 1994). The time-dependent mechanical behavior of rock mass directly affects normal operation and long-term safety of geotechnical engineering, and can be described by the creep model which is the key to stability analysis.

With the development of computation technology and analytical methods, numerical simulations combined with creep models are commonly used in geotechnical engineering (Desai and Zhang, 1987; Barla et al., 2008; Ghorbani and Sharifzadeh, 2009; Deng et al., 2014), for description of the time-dependent deformation of rock mass. The long-term stability of excavations can be evaluated qualitatively using empirical indices such as plastic zone (Zhang et al., 2010), creep damage zone (Chen et al., 2006), excavation damaged zone (Golshani et al., 2007). It is obvious that, at present, strict and quantitative indices are deficient in evaluating the long-term stability of excavations, and the unified and definite stability criteria are also rarely reported. One of the main reasons is probably that the conventional creep models based on rheology can merely consider the time-dependent behavior, and they can hardly describe the intrinsic energy change of material system in time-dependent mechanical processes, which is closely connected to the stability state of materials.

Thermodynamics with internal state variables (ISVs) proposed by Rice (1971) is a powerful method to construct the appealing constitutive equations (Horstemeyer and Bammann, 2010). The models based on thermodynamics with ISVs are thermodynamically consistent and can characterize the intrinsic energy dissipation process and physical changes of microstructure of materials (Lubliner, 1972; Park et al., 1996; Zhu and Sun, 2013). Thus, various researchers develop creep constitutive equations (Chaboche, 1997; Schapery, 1999; Voyiadjis and Zolochevsky, 2000; Challamel et al., 2005; Voyiadjis et al., 2011) based on thermodynamics with ISVs.

Jinping I hydropower station is located on Yalong River in Sichuan Province, China, and it is the topmost concrete arch dam in the world at present. The excavation height of left abutment slope is about 530 m, and the excavation volume is approximately 5.5 million cubic meters, one of the slope projects with the highest excavation height, the largest scale of excavation, and the worst geological condition in China (Xue et al., 2012). The monitoring data showed that the time-dependent deformation of the left abutment slope occurred after excavation (Wang et al., 2014).

* Corresponding author. Tel.: +86 10 62781760.
E-mail address: zhanglong2010@tsinghua.org.cn (L. Zhang).
Peer review under responsibility of Institute of Rock and Soil Mechanics, Chinese Academy of Sciences.

http://dx.doi.org/10.1016/j.jrmge.2015.08.010
1674-7755

In this paper, a creep model with damage, which has been developed by Zhang et al. (2014a, b), is briefly introduced at first. Then the creep model is introduced to FLAC^{3D} (Itasca, 2003) and two calculation codes called CTV-E and CTV-P are developed, respectively. The changes of deformation and stress of dam body, caused by time-dependent deformation of the left bank abutment slope, are explored. Long-term stability of the left bank abutment slope is evaluated by integral curves of energy dissipation rate in domain and its derivative with respect to time. The non-equilibrium evolution rules and the characteristic time are also determined through these curves. Meanwhile, it is indicated that more attention should be paid to some weak regions, where relatively large energy dissipation rates are observed within the slope in the long-term deformation process.

2. Creep model with damage

In the creep model, total strain ε_{ij} is divided into elastic strain ε_{ij}^{e}, viscoelastic strain ε_{ij}^{ve} and viscoplastic strain ε_{ij}^{vp}, i.e.

$$\varepsilon_{ij} = \varepsilon_{ij}^{e} + \varepsilon_{ij}^{ve} + \varepsilon_{ij}^{vp} \tag{1}$$

where

$$\varepsilon_{ij}^{e} = C_{ijkl}\sigma_{kl} \tag{2}$$

$$\eta_e \dot{\varepsilon}_{ij}^{ve} + B\varepsilon_{ij}^{ve} = \frac{\partial A}{\partial \sigma_{ij}} A \tag{3}$$

$$\dot{\varepsilon}_{ij}^{vp} = \frac{\partial f_1^p}{\partial \sigma_{ij}}\dot{\lambda}_1 + \frac{\partial f_2^p}{\partial \sigma_{ij}}\dot{\lambda}_2 + \frac{\partial f_s}{\partial \sigma_{ij}}\dot{\chi} \tag{4}$$

Eq. (2) is the elastic constitutive equation, in which C_{ijkl} is the fourth-order compliance tensor, and σ_{kl} is the stress tensor. Eq. (2) can be rewritten under the hypothesis of isotropy as

$$\varepsilon_m^{e} = \sigma_m/(3K), \quad e_{ij}^{e} = s_{ij}/(2G) \tag{5}$$

where K is the elastic bulk modulus, G is the elastic shear modulus, ε_m^e is the elastic volumetric strain, σ_m is the volumetric stress, e_{ij}^e is the elastic deviator strain, and s_{ij} is the deviator stress.

Eq. (3) is the viscoelastic constitutive equation, in which η_e is the viscoelastic coefficient of viscosity, B is the material constant in Pa, and A is a scalar function of stress. Specially, if we have

$$A = a\sqrt{s_{ij}s_{ij}/2} \tag{6}$$

then Eq. (3) can be rewritten as

$$s_{ij} = 2\eta_1 \dot{e}_{ij}^{ve} + 2G_1 e_{ij}^{ve} \tag{7}$$

where $\eta_1 = \eta_e/a^2$, $G_1 = B/a^2$, a is a parameter, and e_{ij}^{ve} is the viscoelastic deviator strain. Obviously, the viscoelastic volumetric strain ε_m^{ve} can be written as

$$\varepsilon_m^{ve} = 0 \tag{8}$$

In fact, Eq. (3) is based on the kinetic equation of an internal variable, i.e.

$$\dot{\xi} = \frac{1}{\eta_e} f_e = \frac{1}{\eta_e}(A - B\xi) \tag{9}$$

where ξ is an ISV to describe the structure rearrangement in viscoelastic process, and f_e is the thermodynamic force conjugated to the variable ξ (Zhang et al., 2014a).

Eq. (4) is the viscoplastic constitutive equation, in which λ_1 and λ_2 are the macroscopic internal variables used for describing the intrinsic structure rearrangement in viscoplastic response; χ is used to account for the damage effect and other high-energy structure changes; f_1^p, f_2^p and f_s are the thermodynamic forces conjugated with internal variables, and they are all scalar functions of stress and internal variables. In this context, the following assumptions are made:

$$f_1^p = \sqrt{J_2} \tag{10}$$

$$f_2^p = (1 + b\chi)\left(cI_1 + \sqrt{J_2}\right) \tag{11}$$

$$f_s = b\lambda_2\left(cI_1 + \sqrt{J_2}\right) \tag{12}$$

where I_1 is the first invariant of stress tensor, J_2 is the second invariant of deviatoric stress tensor, and b and c are the material parameters. From Eqs. (4) and (10)–(12), we can obtain the following equations:

$$\dot{\varepsilon}_m^{vp} = c\left[(1 + b\chi)\dot{\lambda}_2 + b\lambda_2\dot{\chi}\right] \tag{13}$$

$$\dot{e}_{ij}^{vp} = \left[\dot{\lambda}_1 + (1 + b\chi)\dot{\lambda}_2 + b\lambda_2\dot{\chi}\right]\frac{s_{ij}}{2\sqrt{J_2}} \tag{14}$$

where ε_m^{vp} is the viscoplastic volumetric strain, and e_{ij}^{vp} is the viscoplastic deviator strain.

It is clear that the rate of viscoplastic strain is controlled by the evolution of ISV. We assume the evolutions of λ_1, λ_2 and χ as follows:

$$\dot{\lambda}_1 = \frac{1}{\eta_{p1}}\langle f_1^p - h\lambda_1\rangle \tag{15}$$

$$\dot{\lambda}_2 = \kappa_{p2}\left\langle\frac{f_2^p - R}{R}\right\rangle^p \tag{16}$$

$$\dot{\chi} = \kappa_{p3}\exp(m\chi)\left(\frac{f_s}{R}\right)^2 \tag{17}$$

where η_{p1}, κ_{p2} and κ_{p3} are all viscosity coefficients; m, h, p and R are the material constants; and the symbol $\langle\bullet\rangle$ is the Macaulay bracket. Consider Eq. (11), the following equation is obtained:

$$F = cI_1 + \sqrt{J_2} - \overline{R}, \quad \overline{R} = R/(1 + b\chi) \tag{18}$$

It is clear that Eq. (18) is similar to the Drucker–Prager (D–P) yield criterion. Only when F is larger than 0, the ISV λ_2 will increase. In fact, Eq. (18) can only describe the shear-compression case, thus the creep under tension condition should also be considered. For this, the following tension criterion is adopted:

$$G = \sigma_m - \sigma^{vt} = 0 \tag{19}$$

where σ^{vt} is the material coefficient like tensile strength. Using Eqs. (18) and (19), the domains used in definition of evolution equations are plotted in Fig. 1.

In Fig. 1, the criteria $F = 0$ and $G = 0$ are sketched in $(\sqrt{J_2}, \sigma_m)$ plane. The intersection point of $F = 0$ and $G = 0$ is $B1$, and the curve $h_s = 0$, which passes the intersection point $B1$, is defined as

$$\sqrt{J_2} - a^p\sigma_m - \overline{R} + (a^p + c_1)\sigma^{vt} = 0 \tag{20}$$

where $c_1 = 3c$, a^p is the slope of the curve $h_s = 0$ and defined as $a^p = \sqrt{1 + c_1^2} - c_1$ in this study.

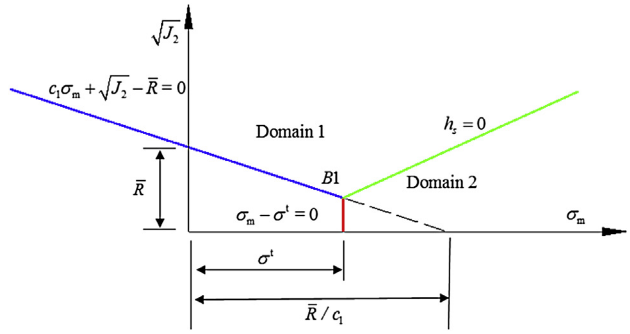

Fig. 1. Domains used in definition of evolution equations.

From Fig. 1, it is known that if the stress is located in Domain 1, the compression will occur, and Eqs. (10)–(12) and (15)–(17) are true. However, if the stress is located in Domain 2, the material is in tension state, and Eqs. (11), (12), (16), (17) should be revised as follows:

$$f_2^{\mathrm{p}} = (1 + b\chi)\sigma_{\mathrm{m}} \tag{21}$$

$$f_{\mathrm{s}} = \frac{\partial f_2^{\mathrm{p}}}{\partial \chi}\lambda_2 = b\lambda_2\sigma_{\mathrm{m}} \tag{22}$$

$$\dot{\lambda}_2 = \kappa_{\mathrm{p2}}\left\langle \frac{f_2^{\mathrm{p}} - \sigma^{\mathrm{vt}}}{\sigma^{\mathrm{t}}} \right\rangle^{\mathrm{p}} \tag{23}$$

$$\dot{\chi} = \kappa_{\mathrm{p3}}\exp(m\chi)\left(\frac{f_{\mathrm{s}}}{T}\right)^2 \tag{24}$$

In this state, the viscoplastic strain rate can also be derived:

$$\dot{\varepsilon}_{\mathrm{m}}^{\mathrm{vp}} = (1 + b\chi)\dot{\lambda}_2 + b\lambda_2\dot{\chi} \tag{25}$$

$$\dot{e}_{ij}^{\mathrm{vp}} = \frac{s_{ij}}{2\sqrt{J_2}}\dot{\lambda}_1 \tag{26}$$

The values of the ISVs can be calculated by evolution equations, and the stress, strain and thermodynamic forces can be determined. The energy dissipation rate Φ can be obtained by

$$\Phi = f_{\mathrm{e}}\dot{\xi} + f_1^{\mathrm{p}}\dot{\lambda}_1 + f_2^{\mathrm{p}}\dot{\lambda}_2 + f_{\mathrm{s}}\dot{\chi} \tag{27}$$

The energy dissipation rate can be used to analyze the stability of sample and to describe the local failure in creep process. The larger the energy dissipation rate, the greater the energy dissipation, and the easier the sample to damage. The integral value of energy dissipation rate in the entire volume domain Ω and its time derivative $\dot{\Omega}$ can also be used to analyze the long-term stability of structure:

$$\Omega = \int_V \Phi \mathrm{d}V = \int_V \left(f_{\mathrm{e}}\dot{\xi} + f_1^{\mathrm{p}}\dot{\lambda}_1 + f_2^{\mathrm{p}}\dot{\lambda}_2 + f_{\mathrm{s}}\dot{\chi}\right)\mathrm{d}V \tag{28}$$

3. Program implementation of creep model

This creep model can be introduced to FLAC^{3D} software for numerical simulations in geotechnical engineering. Firstly, the constitutive equations in rate form (Eqs. (3) and (4)) should be rewritten in central-difference form. According to the increment in total strain, the stress, strain and ISVs can all be updated. If the viscoplasticity is ignored, the constitutive equation in central-difference form can be written as

$$s_{ij}^{\mathrm{n}} = \frac{1}{M}\left[\Delta e_{ij} - \left(\frac{D}{C} - 1\right)e_{ij}^{\mathrm{o-ve}} + Ns_{ij}^{\mathrm{o}}\right] \tag{29}$$

$$\sigma_{\mathrm{m}} = \sigma_{\mathrm{m}}^{\mathrm{o}} + 3K\Delta\varepsilon_{\mathrm{m}} \tag{30}$$

where

$$C = 1 + \frac{G_1\Delta t}{2\eta_1},\ D = 1 - \frac{G_1\Delta t}{2\eta_1} \tag{31}$$

$$M = \frac{1}{2G} + \frac{\Delta t}{4\eta_1 C},\ N = \frac{1}{2G} - \frac{\Delta t}{4\eta_1 C} \tag{32}$$

where the superscripts "n" and "o" denote the new value and the old value over a time step Δt, respectively. When the new stress is obtained, the viscoelastic deviator strain and ISV ξ can be calculated as

$$e_{ij}^{\mathrm{n-ve}} = \frac{1}{C}\left[De_{ij}^{\mathrm{o-ve}} + \frac{\Delta t}{4\eta_1}\left(s_{ij}^{\mathrm{n}} + s_{ij}^{\mathrm{o}}\right)\right] \tag{33}$$

$$\xi^{\mathrm{n}} = \frac{1}{C}\left(D\xi^{\mathrm{o}} + \frac{\Delta t}{a\eta_{\mathrm{e}}}\sqrt{\bar{J}_2}\right) \tag{34}$$

where

$$\bar{J}_2 = \frac{1}{2}\bar{s}_{ij}\bar{s}_{ij},\ \bar{s}_{ij} = \frac{1}{2}\left(s_{ij}^{\mathrm{n}} + s_{ij}^{\mathrm{o}}\right) \tag{35}$$

If the viscoelastic deviator strain is ignored, the constitutive equation in central-difference form can be written as

$$s_{ij}^{\mathrm{n}} = 2G\left(\Delta e_{ij} - \Delta e_{ij}^{\mathrm{vp}}\right) + s_{ij}^{\mathrm{o}} \tag{36}$$

$$\sigma_{\mathrm{m}}^{\mathrm{n}} = \sigma_{\mathrm{m}}^{\mathrm{o}} + 3K(\Delta\varepsilon_{\mathrm{m}} - \Delta\varepsilon_{\mathrm{m}}^{\mathrm{vp}}) \tag{37}$$

The increment in viscoplastic strain is the function of new stress and old stress, and the iterative approach should be adopted to solve Eqs. (36) and (37).

FLAC^{3D} is a three-dimensional explicit finite-difference program for engineering mechanics computation. The user-defined constitutive equation can be written in C++ language and complied as DLL (dynamic link library) files that can be loaded in FLAC^{3D}. In this paper, two new codes (i.e. two DLL files) are developed based on Eqs. (29)–(32) and Eqs. (36) and (37), respectively, called CTV-E and CTV-P. Both names imply the two codes are developed for solving the viscoelastic and viscoplastic problems, respectively.

4. Case study

4.1. Geomechanical model and parameters

The geomechanical model contains six types of rock masses and various faults, such as f_2, f_5, f_8, f_w and lamprophyre vein X. The simulated range of the model is 500 m upstream, 1000 m downstream, 400 m deep under the riverbed, 315 m above the dam crest and 800 m sideways at each side. The geomechanical model is shown in Fig. 2.

The uniform stress is about 5.88 MPa applied on the top surface of meshes to simulate the overburden of rock mass. Other sides of the model except the top are all normally constrained. First, the

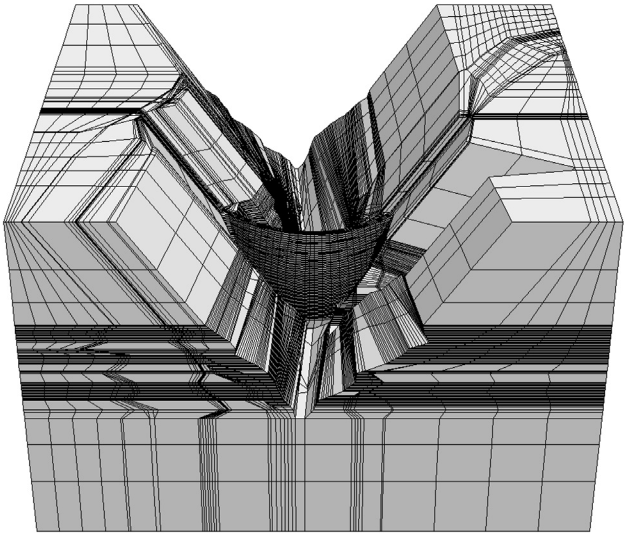

Fig. 2. Geomechanical model of Jinping I hydropower station.

stress and deformation fields under natural condition are calculated. Then, the equilibrium state is obtained under condition of arch dam deadweight. Finally, the normal water load is applied and the equilibrium state is calculated. These computations are based on D-P model considering elastoplasticity, and the deformation and strength parameters are listed in Table 1.

The deformation field of the model is eliminated before the next cycle of computation. The rheological computation is adopted for the materials of the left bank abutment slope. According to Wang et al. (2014), some materials within the left bank slope, like type II rock, type III_1 rock and lamprophyre vein X below 1680 m, are considered to be viscoelastic and the rest are viscoplastic. The calculation code for viscoelastic materials is CTV-E and that for viscoplastic materials is CTV-P. The calculation parameters of viscoelasticity and viscoplasticity are listed in Tables 2 and 3,

Table 1
Deformation and strength parameters.

Material	Elastic modulus, E (GPa)	Poisson's ratio, ν	Unit weight (kN m^{-3})	Friction coefficient, f	Cohesion, c' (MPa)
Concrete of dam body	24	0.167	24	1.7	5
Dam fillet	21	0.167	24	1.35	2
Cushion of dam	21	0.167	24	1.35	2
Type II rock	26	0.25	28	1.35	2
Type III_1 rock	11.5	0.25	28	1.07	1.5
Type III_2 rock	6.5	0.3	28	1.02	0.9
Type IV_1 rock	3	0.35	27.5	0.7	0.6
Type IV_2 rock	2	0.35	27.5	0.6	0.4
Type V_1 rock	0.375	0.35	27.5	0.3	0.02
Type III_1 rock with grouting	12.5	0.25	28	1.07	1.5
Type III_2 rock with grouting	7	0.3	28	1.02	0.9
Type IV_1 rock with grouting	4.25	0.35	27.5	0.7	0.6
Type IV_2 rock with grouting	4.25	0.35	27.5	0.6	0.4
Concrete replacement	21	0.167	24	1.35	2
f_2	0.375	0.35	26	0.3	0.02
f_5 (above 1680 m)	0.375	0.35	26	0.3	0.02
f_5 (below 1680 m)	6.5	0.3	26	1.02	0.9
f_8	0.375	0.35	26	0.3	0.02
$f_{42\text{-}9}$	0.375	0.35	26	0.3	0.02
f_{lc13}	0.375	0.35	26	0.3	0.02
f_{13}	0.375	0.35	26	0.3	0.02
f_{14}	0.375	0.35	26	0.3	0.02
f_{18}	0.375	0.35	26	0.3	0.02
X (above 1680 m)	2	0.35	27.5	0.6	0.4
X (below 1680 m)	6.5	0.3	28	1.02	0.9

Table 2
Calculation parameters of viscoelasticity.

Material	a	G (GPa)	K (GPa)	B (GPa)	η_e (10^7 GPa s)
Type II rock	1	17.33	10.40	120.00	51.84
Type III_1 rock	1	7.67	4.60	106.67	34.56
Type III_2 rock	1	5.42	2.50	66.67	21.60
Type IV_1 rock	1	3.33	1.11	33.33	17.28
Type IV_2 rock	1	2.22	0.74	16.67	8.64
Type III_1 rock with grouting	1	8.33	5.00	106.67	34.56
Type III_2 rock with grouting	1	5.83	2.69	66.67	21.60
Type IV_1 rock with grouting	1	4.72	1.57	33.33	17.28
Type IV_2 rock with grouting	1	4.72	1.57	16.67	8.64
Concrete replacement	1	10.51	9.00	120.00	51.84
X (below 1680 m)	1	5.42	2.50	33.33	17.28

Table 3
Calculation parameters of viscoplasticity.

Material	G (GPa)	K (GPa)	h (GPa)	η_{p1} (10^7 GPa s)	a	R (kPa)	κ_{p2} (10^{-14} s^{-1})
Type V_1 rock	0.14	0.42	0.67	4.32	0.11	22.3	2.58
Faults	0.14	0.42	0.74	0.89	0.11	22.3	2.58
X (above 1680 m)	2.22	0.2	0.2	0.89	0.11	22.3	25.8

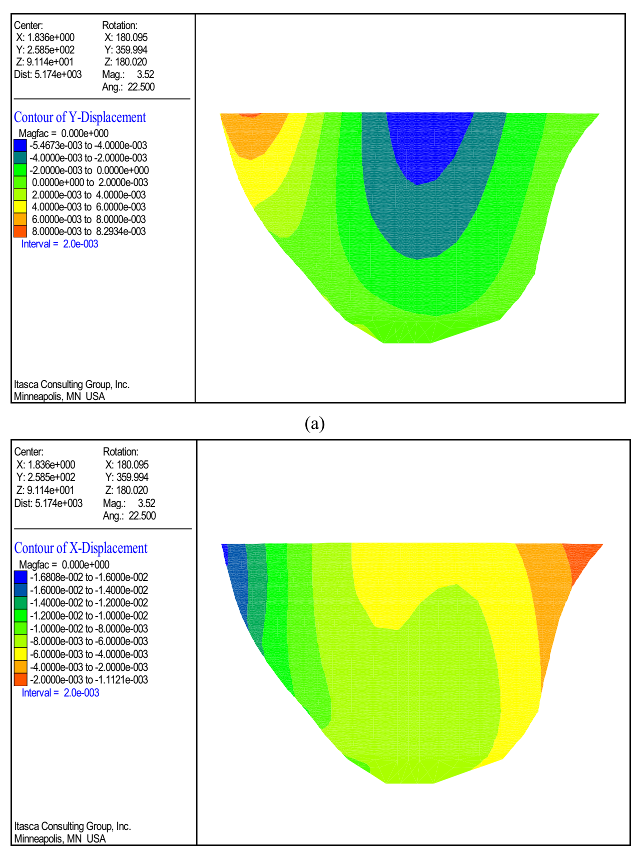

Fig. 3. Contour diagrams of increment in displacement of dam body (displacement unit: m). (a) Along the river. (b) Across the river.

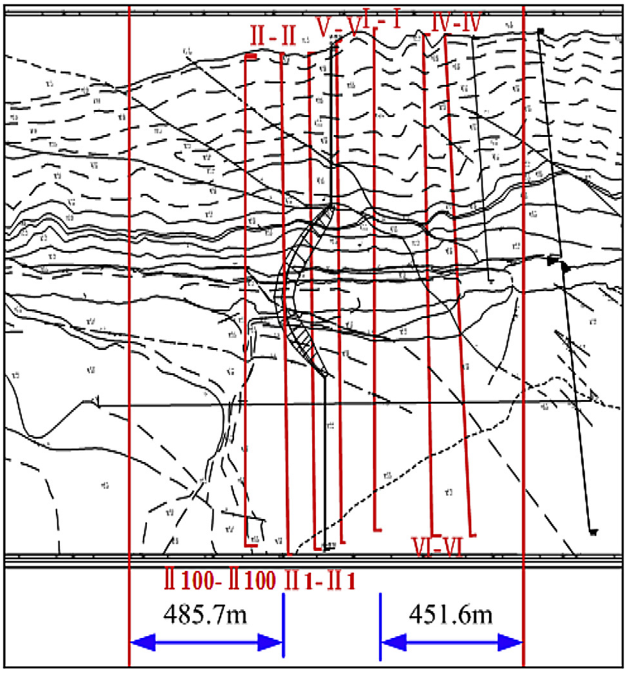

Fig. 4. Location of five sections across the river.

respectively. The damage is excluded here. The duration of rheological computation is 20 years after normal impounding water. The elastoplasticity computation is still adopted for the materials of dam body, fillet, cushion and right bank abutment. The joints of rock mass are not considered and the pore pressure and seepage are also ignored.

4.2. Results and analysis

Under normal water level, the stress and deformation of dam are obtained by elastoplasticity computation in FLAC^{3D}. The maximum principal tensile and compressive stresses are 1.87 MPa and 17.74 MPa, respectively. The largest displacement of dam moving downstream is 60.02 mm at the middle of crown cantilever. The largest displacement across the river is 16.8 mm at left cantilever and towards the valley. After 20 years, the maximum principal tensile and compressive stresses of dam body are 1.27 MPa and 17.81 MPa, respectively. The tensile stress concentration is reduced effectively. The contour diagrams of the increment in displacement for dam body are shown in Fig. 3. It can be seen that the largest increment in displacement moving downstream is 8.29 mm, and that across the river is 16.8 mm towards the right bank.

Table 4
Deformations across the river after 20 years of impounding.

Elevation (m)	Deformations across the river (mm)				
	I–I	V–V	II_1–II_1	II–II	II_{100}–II_{100}
2055	10.47	7.71	8.27	6.15	4.25
1955	12.15	6.84	6.64	9.2	5.41
1885	26.06	15.86	19.74	16.81	18.14
1840	18.52	15.62	17.22	21.42	10.94
1795	17.23	13.39	17.51	16.69	12.91
1750	20.33	15.07	12.36	13.26	13.16
1705	18.27	15.64	10.94	13.38	13.33
1660	18.32	12.03	6.39	8.343	14.95
1610	5.049	10.2	9.65	8.017	11.57

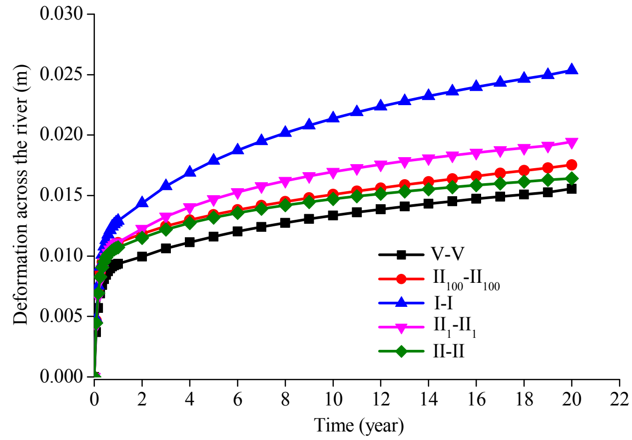

Fig. 5. Time-history curves of deformations of surface points on the crest.

There are five sections across the river, i.e. I–I, V–V, II_1–II_1, II–II, and II_{100}–II_{100}. The y-coordinates of the five sections are 78.1 m, 161.6 m, 78.2 m, −4.8 m and −104.2 m, respectively. The locations of these sections are represented in Fig. 4. Table 4 lists the deformation across the river of the left bank slope at different elevations. It is shown that the deformations of surface points on the crest are almost the largest. Fig. 5 shows the time-history curves of deformations of surface points on the crest.

The long-term stability state of left bank abutment slope can be characterized by Ω–t curve and $\dot{\Omega}-t$ curve, as shown in Fig. 6. It is clear that the left bank slope is asymptotic stable globally after

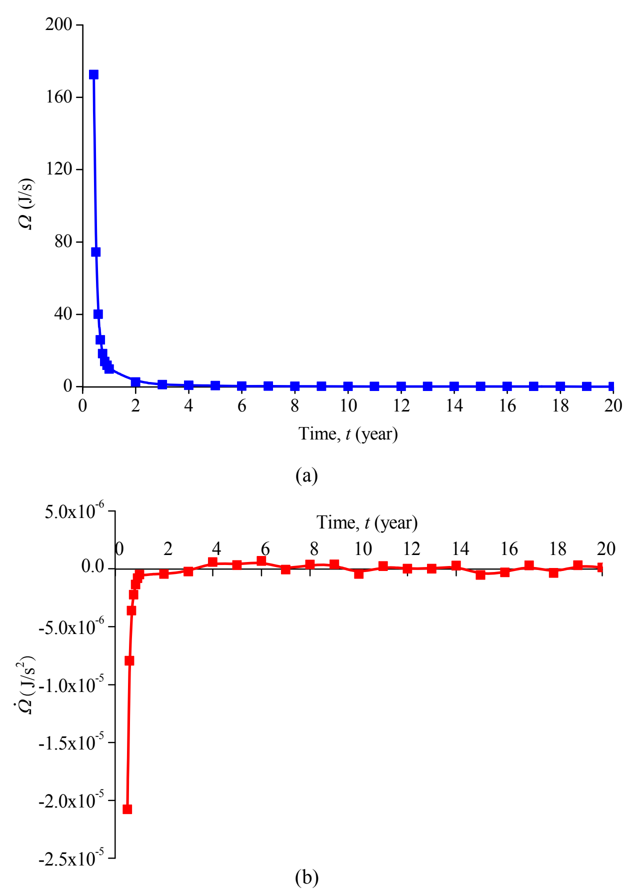

Fig. 6. Ω-t curve and $\dot{\Omega}$-t curve.

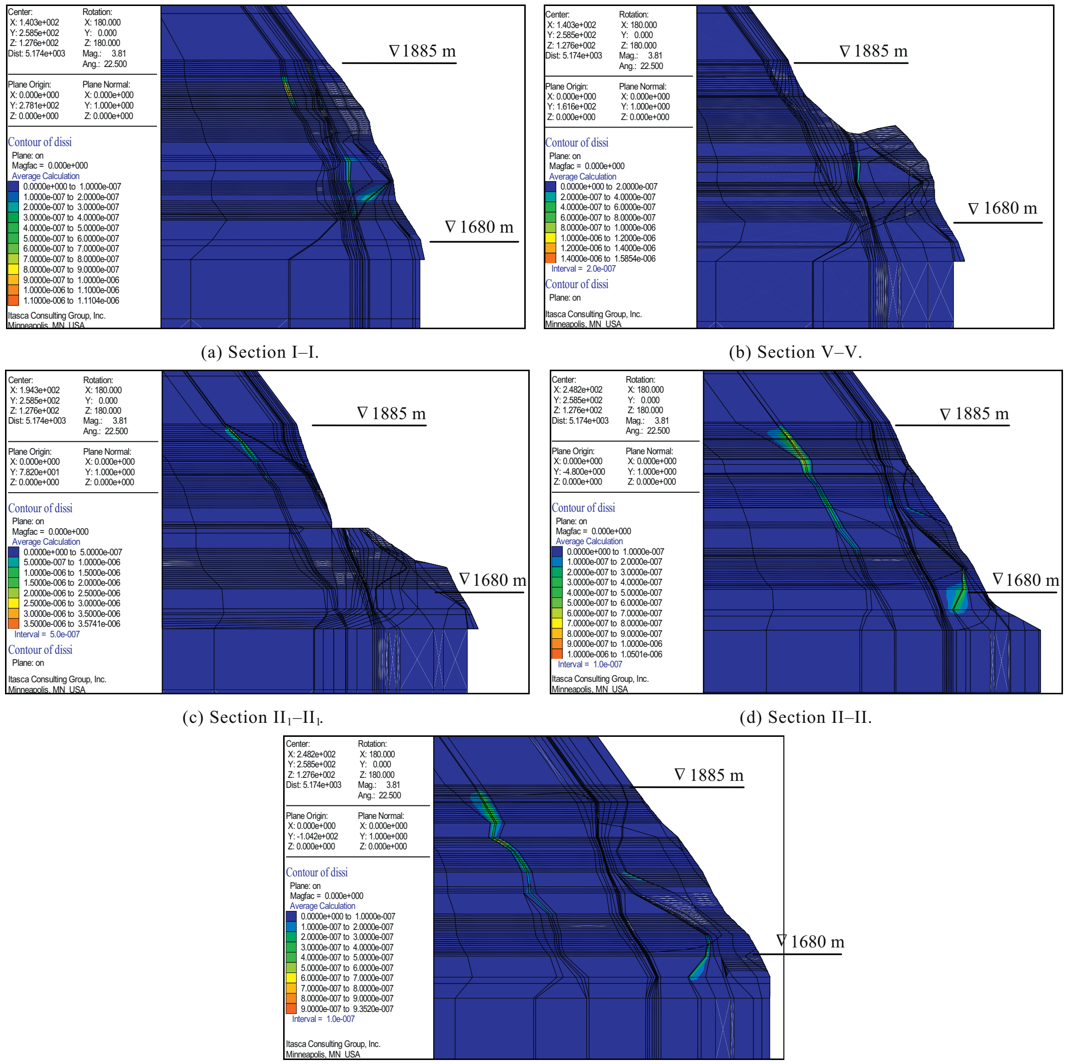

(a) Section I–I.

(b) Section V–V.

(c) Section II_1–II_1.

(d) Section II–II.

(e) Section II_{100}–II_{100}.

Fig. 7. Contour diagrams of energy dissipation rate of five sections.

impounding, and almost reaches the stable state after 3 years of impounding as the values of Ω and $\dot{\Omega}$ are all almost equal to zero.

Fig. 7 shows the contour diagrams of energy dissipation rate of five sections across the river. Although the slope almost reaches global stable state after 3 years of impounding, energy dissipation also occurs in some areas within the slope. These areas may be the weak regions of the slope in the long-term deformation process, and the energy dissipation of these regions could be the internal source of persistent deformation of slope as shown in Fig. 5. The areas with energy dissipation in Fig. 7 are the lamprophyre vein X and fault f_2.

5. Conclusions

The long-term stability of the left bank abutment slope at Jinping I hydropower station is studied using the creep model proposed by the authors. This creep model is based on the thermodynamics with ISVs and introduced into $FLAC^{3D}$. The calculation codes CTV-E and CTV-P are developed and applied to the numerical simulations. The results show that the time-dependent deformation of the left slope can release concentrated tensile stress from the dam body effectively and increase the dam body deformation obviously. After impounding, the left bank tends globally to stable state along with persistent deformation. The lamprophyre vein X and fault f_2 may be the weak regions within the slope in the long-term deformation process.

Conflict of interest

We wish to confirm that there are no known conflicts of interest associated with this publication and there has been no significant financial support for this work that could have influenced its outcome.

References

Barla G, Bonini M, Debernardi D. Time dependent deformation in squeezing tunnels. In: Proceedings of the 12th International Conference of International Association for Computer Methods and Advances in Geomechanics. Goa, India: IACMAG; 2008. p. 4265–75.

Chaboche JL. Thermodynamic formulation of constitutive equations and application to the viscoplasticity and viscoelasticity of metals and polymers. International Journal of Solids and Structures 1997;34(18):2239–54.

Challamel N, Lanos C, Casandjian C. Creep damage modelling for quasi-brittle materials. European Journal of Mechanics – A/Solids 2005;24(4):593–613.

Chen WZ, Wu GJ, Dai YH, Yang CH. Stability analysis of abandoned salt caverns used for underground gas storage. Chinese Journal of Rock Mechanics and Engineering 2006;25(4):848–54 (in Chinese).
Deng JQ, Yang Q, Liu YR. Time-dependent behaviour and stability evaluation of gas storage caverns in salt rock based on deformation reinforcement theory. Tunnelling and Underground Space Technology 2014;42:277–92.
Desai CS, Zhang D. Viscoplastic model for geologic materials with generalized flow rule. International Journal for Numerical and Analytical Methods in Geomechanics 1987;11(6):603–20.
Fakhimi AA, Fairhurst C. A model for the time-dependent behavior of rock. International Journal of Rock Mechanics and Mining Sciences and Geomechanics Abstracts 1994;31(2):117–26.
Ghorbani M, Sharifzadeh M. Long term stability assessment of Siah Bisheh powerhouse cavern based on displacement back analysis method. Tunnelling and Underground Space Technology 2009;24(5):574–83.
Golshani A, Oda M, Okui Y, Takemura T, Munkhtogoo E. Numerical simulation of the excavation damaged zone around an opening in brittle rock. International Journal of Rock Mechanics and Mining Sciences 2007;44(6):835–45.
Horstemeyer MF, Bammann DJ. Historical review of internal state variable theory for inelasticity. International Journal of Plasticity 2010;26(9):1310–34.
Itasca. FLAC^{3D} user's manuals. Minneapolis, USA: Itasca Consulting Group, Inc.; 2003.
Lubliner J. On the thermodynamic foundations of non-linear solid mechanics. International Journal of Non-Linear Mechanics 1972;7(3):237–54.
Park SW, Kim YR, Schapery RA. A viscoelastic continuum damage model and its application to uniaxial behavior of asphalt concrete. Mechanics of Materials 1996;24(4):241–55.
Rice JR. Inelastic constitutive relations for solids – an internal-variable theory and its application to metal plasticity. Journal of the Mechanics and Physics of Solids 1971;19(6):433–55.
Schapery RA. Nonlinear viscoelastic and viscoplastic constitutive equations with growing damage. International Journal of Fracture 1999;97(1–4):33–66.
Voyiadjis GZ, Shojaei A, Li G. A thermodynamic consistent damage and healing model for self-healing materials. International Journal of Plasticity 2011;27(7):1025–44.
Voyiadjis GZ, Zolochevsky A. Thermodynamic modeling of creep damage in materials with different properties in tension and compression. International Journal of Solids and Structures 2000;37(24):3281–303.
Wang RB, Xu WY, Meng YD, Chen HJ, Zhou Z. Numerical analysis of long-term stability of left bank abutment high slope at Jinping I hydropower station. Chinese Journal of Rock Mechanics and Engineering 2014;33(Suppl. 1):3105–13 (in Chinese).
Xue YF, He G, Yang XG, Wu J, Zhou JW. Unloading relaxation and control measures for the high in-situ stress region of left bank slope at Jinping I hydropower station. Journal of Sichuan University: Engineering Science 2012;44(3):55–62 (in Chinese).
Zhang L, Liu YR, Yang Q. A creep model with damage based on internal variable theory and its fundamental properties. Mechanics of Materials 2014a;78:44–55.
Zhang L, Liu YR, Yang Q, Xu LJ. An internal state variable viscoelastic-viscoplastic constitutive equation with damage. Chinese Journal of Theoretical and Applied Mechanics 2014b;46(4):572–81 (in Chinese).
Zhang MH, Gao Q, Zhai SH. Study on creep properties of rock and long-time stability of shaft in high ground stress zone. Chinese Journal of Theoretical and Applied Mechanics 2010;42(3):474–81 (in Chinese).
Zhu H, Sun L. A viscoelastic-viscoplastic damage constitutive model for asphalt mixtures based on thermodynamics. International Journal of Plasticity 2013;40:81–100.

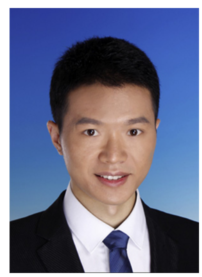

Long Zhang obtained his PhD from Department of Hydraulic Engineering, Tsinghua University, Beijing, China in 2015. Dr. Zhang's research work involves hydraulic structure, geomechanical model test of arch dam, rock mechanics, etc.